



Numerical investigation of the magnetic field effect on the heat transfer and fluid flow of ferrofluid inside helical tube

S. M. Mousavi¹ · N. Jamshidi² · A. A. Rabienataj-Darzi³

Received: 29 June 2018 / Accepted: 1 February 2019 / Published online: 20 February 2019
© Akadémiai Kiadó, Budapest, Hungary 2019

Abstract

The effect of a magnetic field on heat and fluid flow of ferrofluid in a helical tube is studied numerically. The helical tube is under constant wall temperature boundary condition. Parametric studies are done to investigate the effects of different factors such as the magnetic field gradient value and Reynolds number on heat transfer rate and pressure drop. Results indicate that the magnetic field increases the Nusselt number by about 40%. At high magnetic gradient value, Nusselt number and friction factor rise slightly, while at low magnetic gradient value, the increment of Nusselt number is considerable. Furthermore, the growth of wall shear stress on tube wall results in lower thermal–hydraulic performance at the high magnetic gradient value. There is an optimum case for thermal–hydraulic performance which results in most top performance of helical tube in the presence of the magnetic field.

Keywords Helical tube · Ferrofluid · Magnetic field · Thermal–hydraulic performance

List of symbols

Symbols

B	Magnetic field induction (T)
c_p	Specific heat at constant pressure ($\text{J kg}^{-1} \text{K}^{-1}$)
d	Particle diameter (m)
D	Tube diameter (m)
D_c	Coil diameter (mm)
De	Dean number/ $De = Re(DD_c^{-1})^{1/2}$
f	Skin friction factor
G	Magnetic field gradient (A m^{-2})
H	Magnetic field intensity (A m^{-1})
h	Heat transfer coefficient ($\text{W m}^{-2} \text{K}^{-1}$)
J	Electric current density (A m^{-2})
j	Colburn factor

jf	Thermal–hydraulic performance
k	Thermal conductivity ($\text{W m}^{-1} \text{K}^{-1}$)
K_B	Boltzmann constant ($= 1.3806503 \times 10^{-23} \text{ J K}^{-1}$)
L	Langevin function
m	Particle magnetic moment (A m^{-2})
M	Magnetization (A m^{-1})
M_s	Saturation magnetization (A m^{-1})
Nu	Nusselt number/ hDk^{-1}
p_c	Coil pitch (mm)
Pr	Prandtl number
P	Pressure (Pa)
q''	Heat flux (W m^{-2})
Re	Reynolds number
T	Temperature (K)
T_0	Inlet flow temperature (K)
V_{av}	Average velocity at tube cross section (m s^{-1})
$V = (u, v, w)$	Velocity field (m s^{-1})

✉ N. Jamshidi
n.Jamshidi@pnu.ac.ir

¹ Faculty of Mechanical Engineering, Babol University of Technology, Babol, Iran

² Department of Mechanical Engineering, Payame Noor University (PNU), P.O.B. 19395-3697, Tehran, Iran

³ Department of Mechanical Engineering, University of Mazandaran, Babolsar, Iran

Greek letters

μ	Dynamic viscosity ($\text{kg m}^{-1} \text{s}^{-1}$)
μ_0	The magnetic permeability of vacuum ($4\pi \times 10^{-7} \text{ T m A}^{-1}$)
μ_B	Bohr magneton ($= 9.27 \times 10^{-24} \text{ A m}^2$)
ξ	Langevin parameter
ρ	Density (kg m^{-3})

- σ Electrical conductivity (s m^{-1})
 ϕ Particles volume fraction

Superscripts

- f Base fluid
 nf Nanofluid
 p Particle

Introduction

Different types of the tube such as straight, curved and coiled tubes can be used in systems. Centrifugal force in coiled tubes makes secondary flow available in the cross section of tubes and further increases the heat transfer rate. Coiled tubes are used in compact heat exchangers, condensers and evaporators in the food, pharmaceutical, modern energy conversion and power utility systems, heating, ventilating and air conditioning (HVAC) engineering and chemical industries [1–3]. In the last few decades, to save energy and raw materials, and taking into account economic and environmental issues, many efforts have been made to build high-performance heat exchangers, and their primary purpose is to reduce the size of the system for a given heat load and increase the heat transfer capacity. An overview of the work done in this area can be divided into the following general methods: Passive methods that do not require external force and active methods that need external power. In curved tubes, centrifugal force makes a pair of vorticities which is present in the cross section of the tube. Helical tubes are a kind of curved tubes which increase the heat transfer rate in a fixed length of tubes, because of these secondary flows. As helically coiled heat exchangers are widely used in industry, several researchers made efforts to drive correlations for heat transfer rate and pressure drop in helical tubes. Some proposed Nusselt number correlations [4], while others investigate both Nusselt number and friction factor [5–9]. Investigations were also made to enhance the heat transfer rate in these tubes [10, 11], and some used nanofluid as working fluid [12–16] in these tubes. Jamshidi et al. [14] found the optimum coil diameter, coil pitch and flow rates in shell and tube side to enhance the heat transfer rate in helical tube heat exchanger. They found that higher coil diameter, lower coil pitches and higher flow rates in shell and tube sides can be a good choice for these kinds of heat exchangers.

Ferrofluid is called to the suspension of magnetic particles in the conventional heat-carrying fluid. These suspended particles can have the nanometer size. Most conventional ferrofluids are suspensions of iron or cobalt in water or Kerosene. To overcome the attractive van der

Walls forces between nanoparticles, they are covered by a surfactant layer. This layer prevents nanoparticles agglomeration. One of the active techniques to augment heat transfer is using a magnetic field. By the use of the magnetic field, flow and heat transfer by the fluid can be controlled. Magnetic nanofluids can be used in engineering applications to control the heat transfer rate in different sections of systems. Ferrofluids have lower thermal conductivity concerning metal or metal oxide nanofluid, but its controllable characteristics make it an ideal working fluid in thermal systems [17, 18]. Khairul et al. [19] reviewed the recent articles on ferrofluids to compare the reported characteristics of such fluids which are critical to the fluid flow and heat transfer phenomenon. There are several scientific investigations both numerically and experimentally which analyzed the effects of uniform and non-uniform magnetic fields. Abbasi et al. [20] showed that the Kelvin body force affect the vortices around the sphere located in a channel in the presence of a uniform external magnetic field. Vortexes decrease the boundary layer thickness and enhance the heat transfer rate. In addition, average Nusselt number is highly dependent on the magnetic field intensity. Rahman et al. [21] used cobalt-kerosene ferrofluid in a semicircular enclosure to examine the effects of Rayleigh number, nanoparticles volume fraction and Hartmann number on the MHD convective heat transfer rate. They stated that Rayleigh number growth boosts the heat transfer rate; however, increasing magnetic field intensity sets it back. Shafiei et al. [22] numerically studied the results of a non-uniform magnetic field on Fe_3O_4 /kerosene flow in a vertical tube. They used two-phase mixture model in their three-dimensional simulations. They reported that negative magnetic field increases the heat transfer rate and pumping power, while positive gradient causes a decrease in heat transfer and pumping power. Jafari et al. [23] used Taguchi to optimize the thermomagnetic effect in a cylinder. The magnetic Soret effect is dependent on the magnetic field strength. Ghadiri et al. [24] experimentally analyzed Fe_3O_4 -water ferrofluid in a PVT system. They examined the cooling capacity of ferrofluids under constant and alternating magnetic field. They stated that by 3 mass% ferrofluid in the presence of constant and alternating magnetic field, the overall efficiency of system increases 45% and 50%, respectively, in comparison with distilled water. Sadeghinezhad et al. [25] prepared a hybrid nanofluid that consists of graphene oxide- Fe_3O_4 in water and added tannic acid to increase the stability of fluid. The thermal conductivity of Ferrofluid increased by 11%. The test section comprised of a straight tube, and heat transfer rate and pressure drop are obtained from the experimental data. When no magnetic field is applied, heat transfer enhancement is negligible, while in the presence of magnetic field,

heat transfer coefficient increased by 82%. The sinusoidal magnetic field was studied numerically by Fadaei et al. [26] in a channel with constant wall temperature. The effects of parameters such as magnetic field intensity and frequency, fluid inlet velocity and spin viscosity on duct Nusselt number were examined. By increasing ferrofluid inlet velocity, the Nusselt number decreases, while the Nusselt number has an optimum value versus intensity and frequency of magnetic field and spin viscosity. Temperature profiles in the duct are highly dependent on the magnetic field and the type of ferrofluid. Bahiraei and Hangi [27] numerically simulated a double pipe heat exchanger, while the working fluid was Mn–Zn ferrite in the presence of quadrupole magnetic field. The distribution of particles in the tube is more uniform. Both heat transfer and pressure drop are increased as the concentration, the particle size and the magnitude of the magnetic field rise. The optimum values that lead to the optimum case results in more heat transfer and less pressure drop are gained using the genetic algorithm. Mokhtari et al. [28] numerically studied a tube with inserted twisted tape in the presence of a non-uniform magnetic field. The magnetic field results in 30% enhancement in Nusselt number, while increasing nanoparticles volume fraction enhances the thermal performance of tube. When the concentration of nanoparticles grew to more than 2%, no significant change in the heat transfer rate was observed. Using higher pitch size of twisted tape resulted in substantial temperature increase. Yarahmadi et al. [29] experimented to analyze the effects of magnetic field on a circular tube test section. The impact of several magnetic parameters such as magnetic field strength, arrangements, the constancy or oscillation modes on convective heat transfer rate were examined. Higher volume fractions of ferrofluid and lower Reynolds number made more top heat transfer. Oscillating magnetic field leads to about 19.8% enhancement in local convective heat transfer. Ahangar et al. [30] locate quadrupole magnets at different axial positions along a vertical tube. They used $\text{Fe}_3\text{O}_4/\text{water}$ ferrofluid. Maximum enhancement in local heat transfer coefficient was about 48.9% when $\phi = 2\%$. When Reynolds number was equal to 580, the pressure drop increased by 1%. Increasing Reynolds number reduced the heat transfer rate enhancement. Heat transfer in a circular stainless steel tube under constant heat flux in the presence of ferrofluids and the magnetic field was simulated in Comsol by Asfer et al. [31]. They stated that forming the aggregation of chain-like nanoparticles clusters at the wall, affect the heat transfer and under various conditions can increase or decrease the heat transfer rate. Lajvardi et al. [32] experimentally analyzed copper tube. They stated that the main reason for the enhanced heat transfer characteristics of fluid is related to the remarkable change in thermo-physical properties of ferrofluids in the

presence of magnetic fields. Magnetic field effects on curved tubes were studied numerically by Aminifar et al. [33]. They showed that a linear magnetic field helps centrifugal force effects on enhancing the heat transfer augmentation of ferrofluids. Lid-driven cavity under different geometric shapes (lid-driven cavity with flexible side wall [34], cavity with corrugated partition [35], filled cavity with internal heat generation [36], trapezoidal cavity [37] and square cavity with ventilation ports [38, 39]) and a rotating cylinder in the presence of backward facing step [40] was studied for different types of ferrofluids under forced [38, 40], natural [35, 36] and mixed convection [37, 39, 41, 42] heat transfer by Selimfendigil and Oztop. They numerically stated that the length and size of recirculation zones and heat transfer level is substantially affected by magnetic field. In the case of rotating cylinder, the effect of cylinder rotation is more pronounced at low Reynolds numbers; when the magnetic dipole is closer to the bottom wall of cavity, more area of cavity senses the accelerated flow.

Concerning literature review, there are differences in the function of ferrofluids in different systems. Therefore, further investigations can be done in the field of ferrofluids. The effects of different Reynolds numbers and magnetic gradient on average heat transfer rate and wall shear stress in the helical tube are examined numerically in this study.

Theoretical formulation

Governing equations

Three-dimensional, steady, laminar flow of water– Fe_3O_4 nanofluid in a helical tube in the presence of a non-uniform magnetic field is considered. The schematic model of the supposed problem is shown in Fig. 1. The helical tube has a coil diameter, coil pitch and tube diameter equal to $D_c = 0.07$ m, $P_c = 0.0214$ m, $D = 0.012$ m, respectively. The magnetic field intensity (\mathbf{H}) is along the y directions

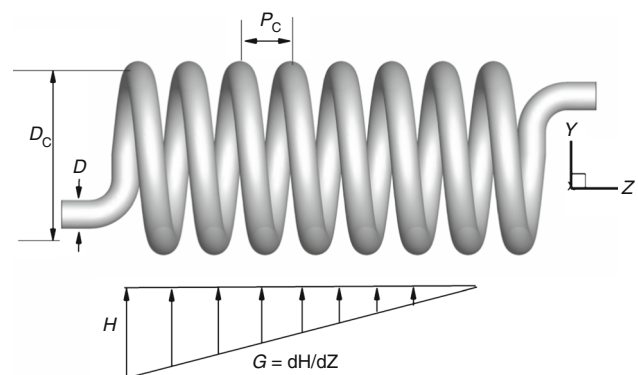


Fig. 1 Geometry of problem and magnetic field applied to the tube

and linearly varies along z -direction with the magnetic field gradient G . The tube inlet and outlet are located at $z = -0.027$ m and $z = 0.1982$ m, while the magnetic field gradient is applied in the range of $0 \text{ m} \leq z \leq 0.15$ m. Critical Reynolds number in helical tubes is higher than straight tubes and is directly dependent on the curvature and it can be estimated by Eq. (1) proposed by Ito [43]:

$$Re_{cr} = 2000(DD_c^{-1})^{3/2} \tag{1}$$

The inlet mass flow rate of ferrofluid are corresponding to $Re = 1500\text{--}6000$, so the flow is laminar in the range of study. The boundary condition in this study can be expressed as:

- At the tube inlet, temperature is constant, $T_0 = 300$ K; while the velocity values are selected in the range of laminar flow, $Re = 1500\text{--}6000$.
- On the tube wall, temperature is fixed at $T = 373.15$ K with no slip boundary condition, $u = 0, v = 0, w = 0$.
- At the tube exit, the gradient of all variables in the normal direction to the tube cross section is set to zero.

The working fluid is 4 vol% fraction Fe_3O_4 -water ferrofluid. The water-based nanofluid consists of Fe_3O_4 spherical shape particles with 10 nm mean diameter. Physical properties of the studied fluid and particles are presented in Table 1 [44]. The nanofluid is assumed to be Newtonian and incompressible. The physical properties of the nanofluid are supposed to be constant. It is expected that the nanoparticles in the base fluid are well dispersed; therefore, the nanofluid is considered homogeneous. Furthermore, it is assumed that the continuous phase and the nanoparticles are in the thermal equilibrium and the slip velocity between them is negligible. By taking expressed assumptions, nanofluid can be considered as a single-phase fluid with physical properties based on the concentrations of two components.

Viscosity changes due to the applied magnetic field are neglected, and equilibrium magnetization (\mathbf{M} and \mathbf{H} parallel) and continuation of magnetic induction, i.e., $\nabla \cdot \mathbf{B} = 0$, are considered. Given the assumptions, based on the principles of ferrohydrodynamics (FHD) [45] and magnetohydrodynamics (MHD) [46], according to Ref. [47], the equations governing the flow are as follows:

Continuity equation:

$$\nabla \cdot V = 0 \tag{2}$$

Momentum equation:

$$\rho_{nf}(V \cdot \nabla)V = -\nabla P + \mu_{nf}\nabla^2V + \mu_0M\nabla H + J \times B \tag{3}$$

Energy equation:

$$(\rho c_p)_{nf}(V \cdot \nabla)T = k_{nf}\nabla^2T - \mu_0T \frac{\partial M}{\partial T}(V \cdot \nabla)H + \frac{J \cdot J}{\sigma_{nf}} \tag{4}$$

The physical properties of the nanofluid can be defined based on the properties of the base fluid and nanoparticle:

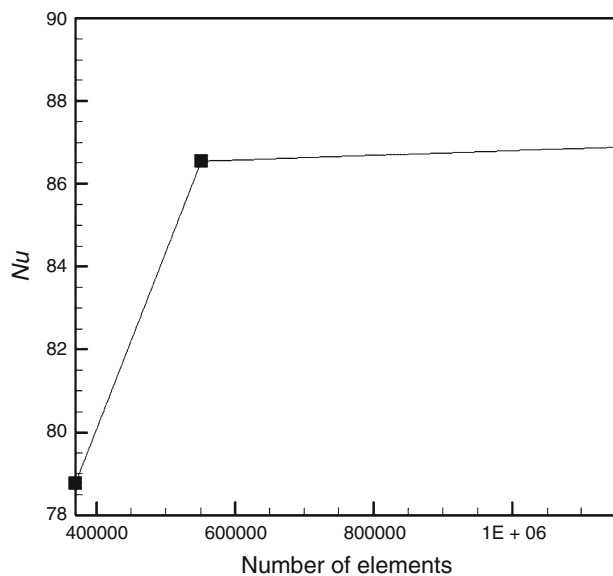


Fig. 2 Grid independency analysis

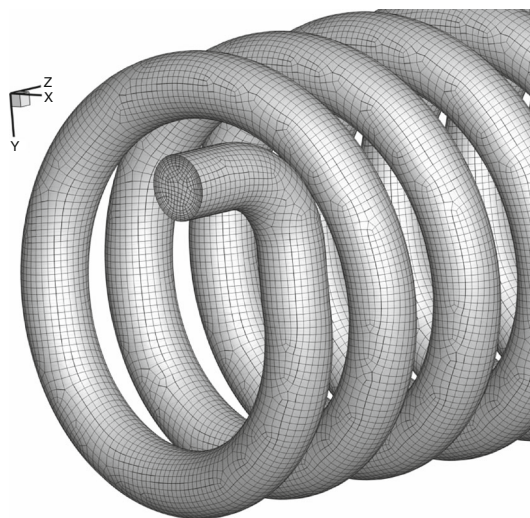


Fig. 3 The grid system applied in numerical procedure

Table 1 Properties of base fluid and particles [44]

	$\rho/\text{kg m}^{-3}$	$\mu/\text{kg m}^{-1} \text{ s}^{-1}$	$c_p/\text{J kg}^{-1} \text{ K}^{-1}$	$k/\text{W m}^{-1} \text{ K}^{-1}$	$\sigma/\text{s m}^{-1}$
Water	998.2	0.001003	4182	0.6	0.05
Fe_3O_4	5200	–	670	6	25,000

The effective density of the nanofluid is determined as [48]

$$\rho_{nf} = (1 - \phi)\rho_f + \phi\rho_p \tag{5}$$

The effective viscosity of the nanofluid is calculated using the Brinkman model [48]

$$\mu_{nf} = \frac{\mu_f}{(1 - \phi)^{2.5}} \tag{6}$$

The heat capacitance of the nanofluid is given as [48]

$$(\rho c_p)_{nf} = (1 - \phi)(\rho c_p)_f + \phi(\rho c_p)_p \tag{7}$$

The effective thermal conductivity of the nanofluid is approximated using the Hamilton and Crosser model [49]

$$k_{nf} = \frac{k_p + (n - 1)k_f - (n - 1)\phi(k_f - k_p)}{k_p + (n - 1)k_f + \phi(k_f - k_p)} k_f \tag{8}$$

where n is the empirical shape factor that is 3 for spherical particles.

The effective electrical conductivity of nanofluid was presented by Maxwell [50] as

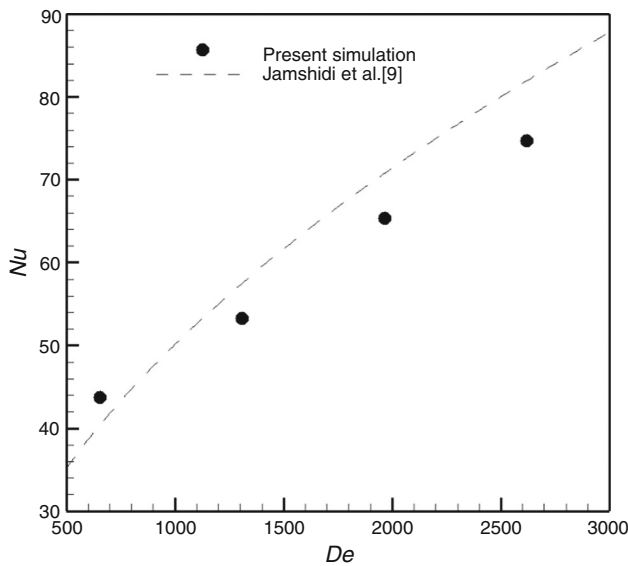


Fig. 4 Validation of numerical procedure

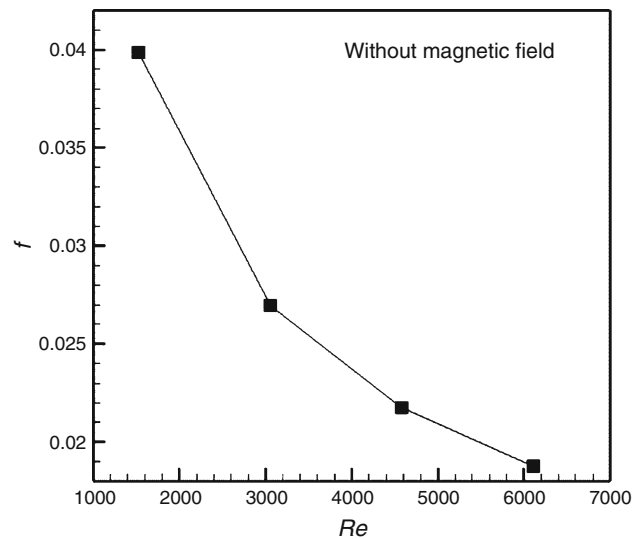


Fig. 6 The effect of Reynolds number on friction factor without magnetic field

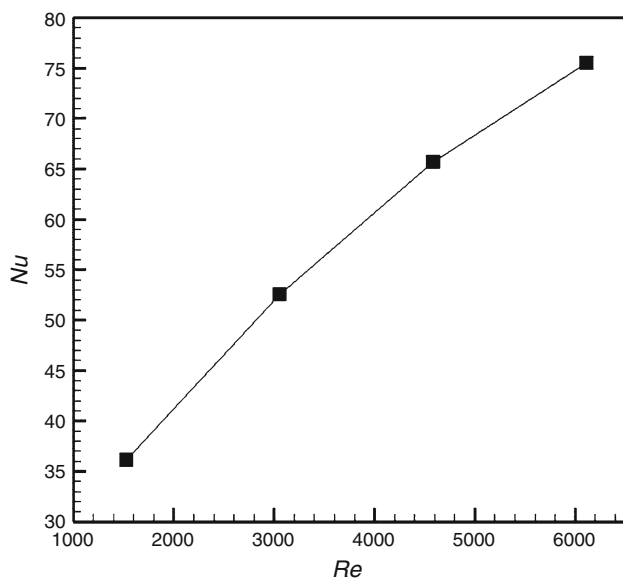


Fig. 5 The effect of Reynolds number on Nusselt number without magnetic field

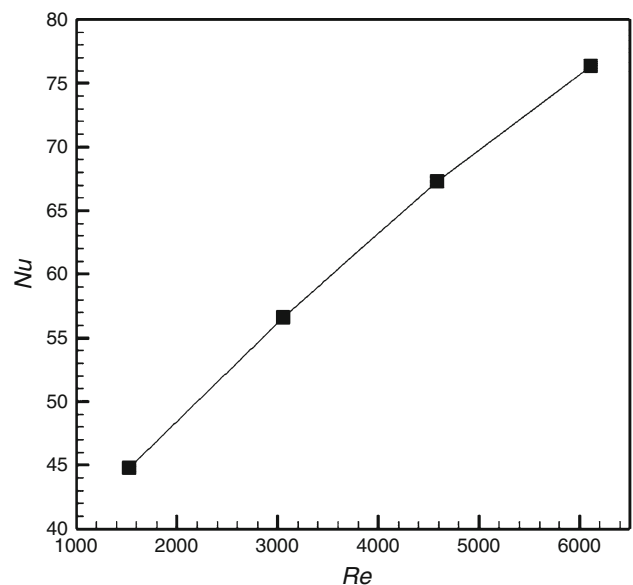


Fig. 7 The effect of Reynolds number on Nusselt number in the presence of magnetic field $G = 2 \times 10^7 \text{ A m}^{-2}$

$$\sigma_{nf} = \left(1 + \frac{3 \left(\frac{\sigma_p}{\sigma_f} - 1 \right) \phi}{\left(\frac{\sigma_p}{\sigma_f} + 2 \right) - \left(\frac{\sigma_p}{\sigma_f} - 1 \right) \phi} \right) \sigma_f \tag{9}$$

In the above equations, $\mathbf{V} = (u, v, w)$ is the velocity field, ρ is the density, P is the pressure, μ is the dynamic viscosity, T is the temperature, μ_0 is the magnetic permeability of vacuum, \mathbf{M} is the magnetization, \mathbf{H} is the magnetic field intensity, \mathbf{J} is the density of the electric current which $\nabla \times \mathbf{H} = \mathbf{J} = \sigma_{nf} (\mathbf{V} \times \mathbf{B})$, \mathbf{B} is the magnetic field induction, c_p is the specific heat at constant pressure, k is the thermal conductivity, σ is the electrical conductivity, and ϕ is the particles volume fraction.

The terms $\mu_0 M \nabla H$ and $\mathbf{J} \times \mathbf{B}$ in Eq. (3) represent the components of the magnetic force per unit volume. $\mu_0 M \nabla H$ is due to magnetization that depends on the existence of the magnetic gradient. $\mathbf{J} \times \mathbf{B}$ represents the Lorentz force per unit volume which is due to the induced electric current.

The terms $\mu_0 T \partial M / T (\mathbf{V} \cdot \nabla) H$ and $\mathbf{J} \cdot \mathbf{J} \sigma_{nf}^{-1}$ in Eq. (4) represent the thermal power per unit volume due to the magnetocaloric effect and the Joule heating, respectively.

The magnetization is defined as follows [51]

$$M = M_s L(\xi) = \frac{6\phi m}{\pi d^3} \left(\cot h(\xi) - \frac{1}{\xi} \right) \tag{10}$$

where M_s is the saturation magnetization, L is Langevin function, m is the particle magnetic moment, d is the particle diameter, and ξ is the Langevin parameter which is defined as

$$\xi = \frac{\mu_0 m H}{k_B T} \tag{11}$$

where k_B is the Boltzmann constant.

The unit cell of the crystal structure of magnetite has a volume of about 730 \AA^3 and contains 8 molecules Fe_3O_4 and each of them have a magnetic moment of $4\mu_B$ [51] where μ_B is the Bohr magneton. Therefore, the particle magnetic moment for the magnetite particles is obtained as [51]:

$$m = \frac{4\mu_B \pi d^3}{6 \times 91.25 \times 10^{-30}} \tag{12}$$

The magnetic field induction is defined as [44]

$$\mathbf{B} = \mu_0 (\mathbf{H} + \mathbf{M}) \tag{13}$$

Numerical method

In the present study, the computational fluid dynamics software, FLUENT, was employed to solve the mentioned equations in the previous section using finite volume methodology. Coupled algorithm and PRESTO

scheme were used for the velocity–pressure coupling and pressure correction equation, respectively. The convective and diffusive terms were discretized by using second-order upwind scheme. To employ the magnetic effects, some User-Defined Functions (UDFs) were written and added to the software.

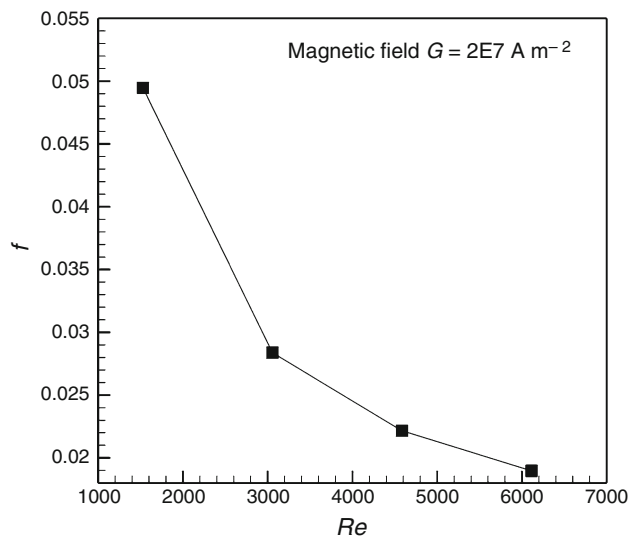


Fig. 8 The effect of Reynolds number on friction factor in the presence of magnetic field $G = 2 \times 10^7 \text{ A m}^{-2}$

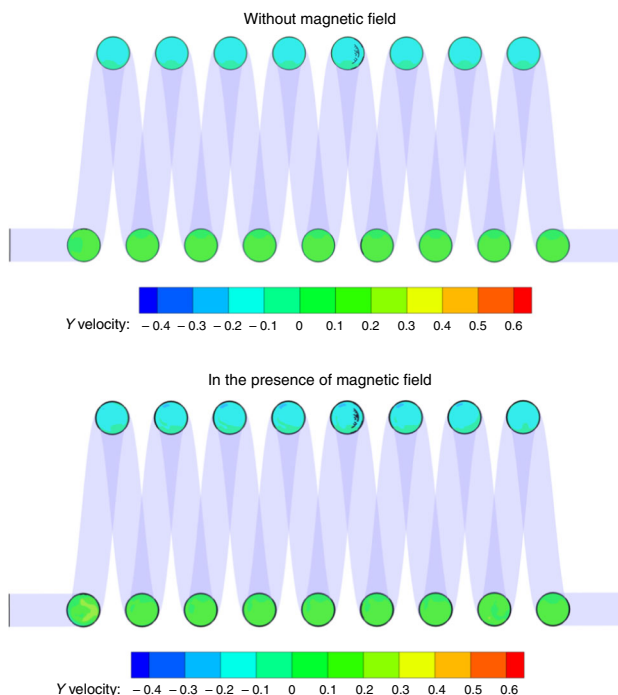


Fig. 9 Velocity contours in the absence (upper) and the presence (lower) of magnetic field

Computational grid

In this section, the verification of grid system and solution procedure is done. Three sets of grid systems are examined for the helical tube. The geometry and operating condition are fixed while the average Nusselt number on the tube wall is compared for three grid systems, and the results are

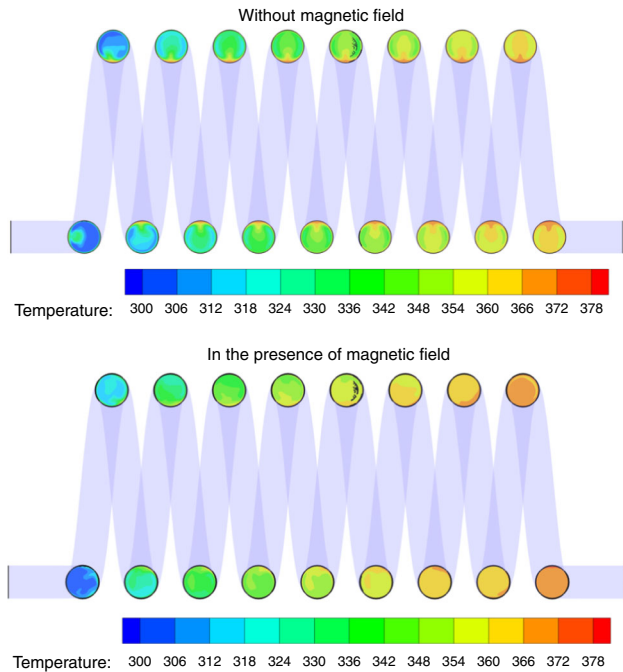


Fig. 10 Temperature contours in the absence (upper) and the presence (lower) of magnetic field

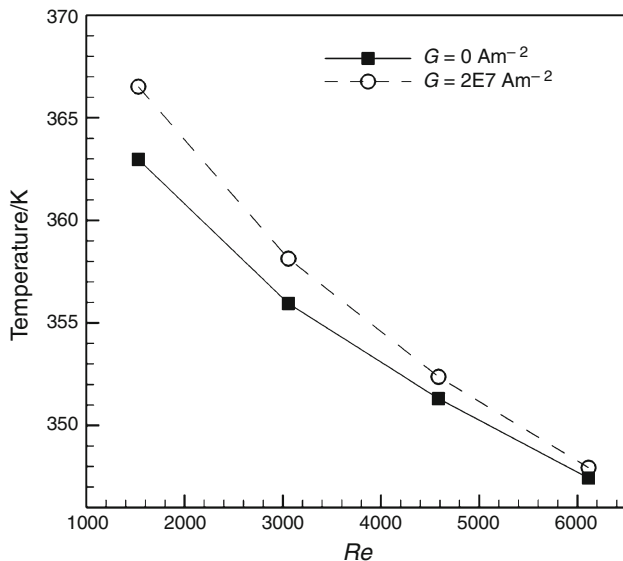


Fig. 11 The effect of Reynolds number and the magnetic field on outlet temperature

presented in Fig. 2. It was observed that the systems with about 550,000 and 1,200,000 cells produce the almost identical Nusselt number, while the precision of solution varied slightly, which can be ignored to reach less computational time. Thus, a domain with 550,000 cells was chosen in the present study. In Fig. 3, the grid system selected for the current numerical study is presented.

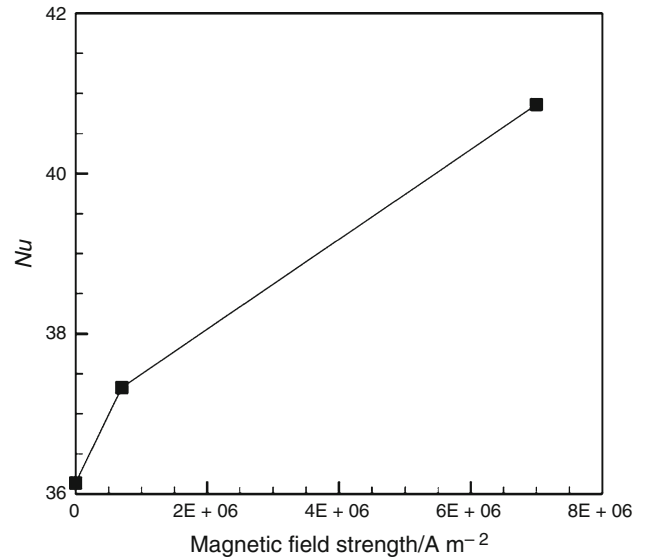


Fig. 12 The effect of the magnetic gradient value on Nusselt number at low field strength ($Re = 1528.36$)

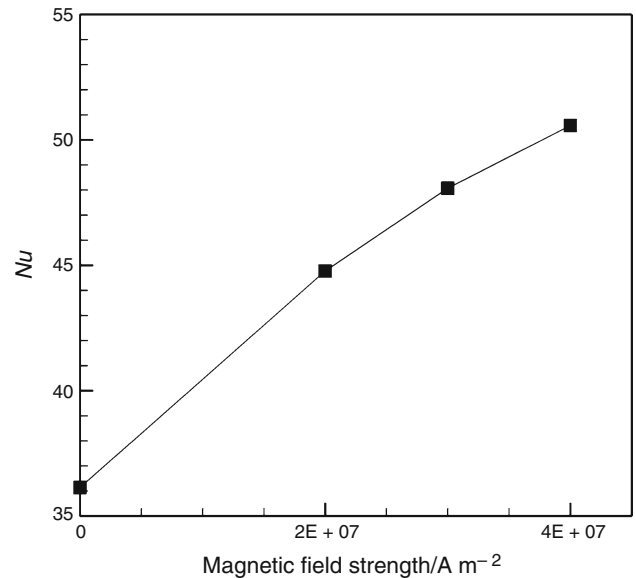


Fig. 13 The effect of the magnetic gradient value on Nusselt number at high field strength ($Re = 1528.36$)

Results

To analyze the accuracy of the numerical method, the simulation results are compared with experimental results reported by Jamshidi et al. [9]. Since the experimental work by Jamshidi et al. [9] is done for water in the helical pipe at laminar flow condition, the same geometry and model are simulated for the validation. The presented results in Fig. 4 reveal that there is a reasonably good agreement between the numerical and experimental results.

The effect of Reynolds number on the Nusselt number is shown in Fig. 5. As Reynolds number increases, the boundary layer thickness decreases, which results in higher heat transfer rate between the tube wall and fluid flow and higher Nusselt number. Figure 6 shows the effect of Reynolds number on wall friction factor. When Reynolds number is 1528, average shear stress on the tube wall is

equal to $\tau = 0.296$ Pa, while at $Re = 6113$, wall shear stress grows to $\tau = 2.232$ Pa. As the fluid properties and tube diameter are fixed, the increase in Reynolds number is only due to the increment of fluid velocity. Although shear stress increases, the higher velocity at higher Reynolds numbers results in lower wall friction factor at high Reynolds number.

Ferrofluid is made by $\phi = 4\%$ volume fractions of Fe_3O_4 nanoparticles in water ferrofluid. Further investigation is done to analyze the effect of magnetic field on the heat transfer phenomenon in the helical tube. Magnetic field gradient equal to $G = 2 \times 10^7$ $A\ m^{-2}$ is applied to the desired section of the tube. The presence of magnetic field can see an upward trend for the Nusselt number as the Reynolds number change (Fig. 7). Friction factor (Fig. 8) has a downward pattern, which is due to the increase in fluid velocity. However, the Nusselt number in a fixed

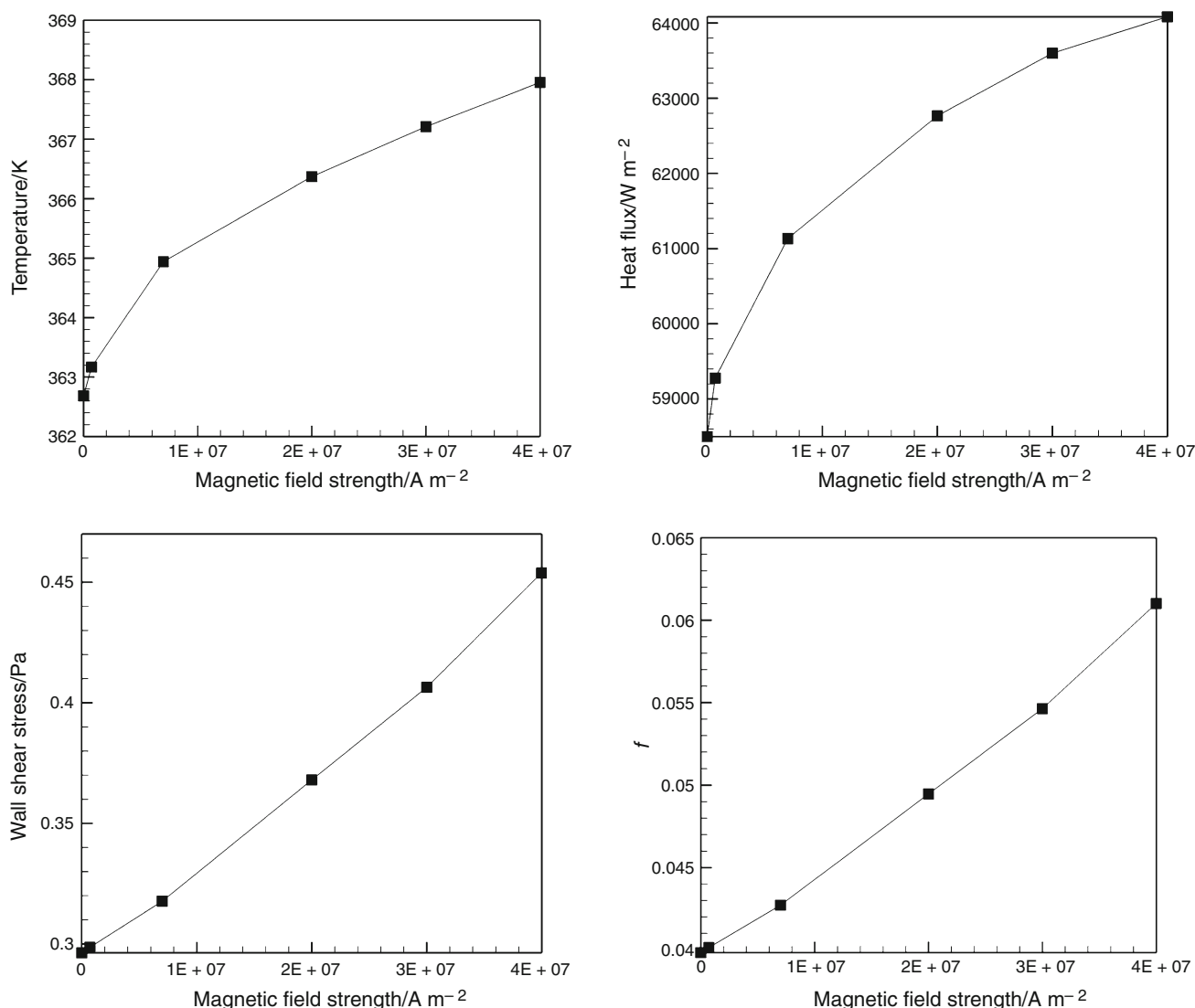


Fig. 14 The effect of the magnetic gradient value on outlet temperature, wall heat flux, shear stress and friction factor

Reynolds number is enhanced by the presence of gradient magnetic field. The magnetic field can change the shape of temperature profile at the tube cross section. In Fig. 9, velocity profiles in the absence and presence of magnetic field ($G = 2 \times 10^7 \text{ A m}^{-2}$) are compared. In this figure, the velocity components at y -direction is depicted, while this velocity component is normal to tube cross sections (iso-surfaces at $y = 0$ in x - z plane). Figure 10 shows the temperature contour at the described sections. At $G = 2 \times 10^7 \text{ A m}^{-2}$, flatter temperature and velocity profiles are available at the tube cross section (Figs. 9, 10); as a result, higher heat transfer rate and pressure drop (Figs. 7, 8) are generated at the tube wall.

In Fig. 11, the temperature at the outlet section of the helical tube decreases by Reynolds number increase. This is because higher Reynolds number means higher fluid velocity, which in turn, results in lower fluid inhabitance time in the tube and lower outlet temperature. The same trend for outlet temperature can be seen in the absence of magnetic field with increasing Reynolds number. Ferrofluid temperature at the outlet of the tube decreases with an increase in Reynolds number.

The effect of magnetic field gradient value on heat transfer rate is depicted in Figs. 12 and 13. The impact of the magnetic field can be divided into two different sections. At low magnetic field gradient, the enhancement in Nusselt number in the presence of magnetic field is sharp, in Fig. 12, while, at the higher magnetic gradient value (Fig. 13), the upward trend is with lower slope. The boundary layer thickness can justify the effect of the magnetic field on heat transfer rate by the presence of magnetic field. It could be concluded that the magnetic forces can increase the Nusselt number by 40% at $Re = 1528.36$. The results indicate that Nusselt number increases by 13%, 24% and 40% for the strength of $G = 7 \times 10^6 \text{ A m}^{-2}$, $G = 2 \times 10^7 \text{ A m}^{-2}$, $G = 4 \times 10^7 \text{ A m}^{-2}$, respectively, in comparison with the tube without magnetic field.

Figure 14 demonstrates the effect of the magnetic gradient value on outlet temperature, heat flux exchange via tube surface, shear stress on the tube wall and skin friction factor. The rise in convection heat transfer coefficient in ferrofluid is related to the ratio of thermal conductivity of ferrofluid to the boundary layer thickness. The higher thermal conductivity of Nanofluids leads to a decrease in boundary layer thickness and changes the temperature profiles at the cross section of the tube. This phenomenon causes a considerable rise in Nusselt number. The presence of magnetic field increases the heat transfer and the shear stress on the tube wall.

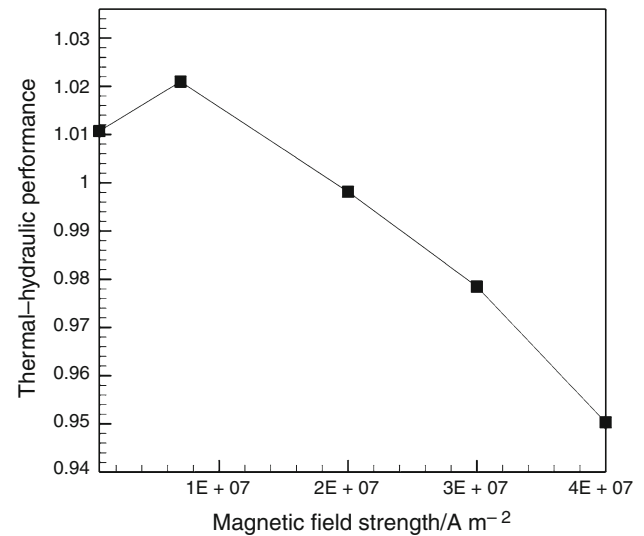


Fig. 15 The effect of the magnetic gradient value on thermal-hydraulic performance of helical tube

To study the thermal and hydraulic behavior of helical tube, jf which is a dimensionless parameter is assessed [52]:

$$jf = j/f^{1/3} \quad (14)$$

where j and f are Colburn and friction factors, respectively, which are defined as:

$$j = \frac{hpr^{2/3}}{\rho c_p V_{av}} \quad (15)$$

$$f = \frac{2D\Delta p}{L\rho V_{av}^2} \quad (16)$$

As illustrated in Fig. 15, thermal hydraulic performance obeys a controversial pattern. It is revealed that at the low magnetic gradient value, the thermal hydraulic performance trend is upward and at $G = 7 \times 10^5 \text{ A m}^{-2}$, the curve has a maximum. It means that higher magnetic gradient value results in lower tube performance. At the higher magnetic gradient value, the increment of shear stress overcomes the heat transfer modification, and tube performance experiences a declining trend after its optimum value.

Conclusions

In this study, using computational fluid dynamics, a coiled tube is simulated. Studies have been done in laminar flow condition under constant wall temperature boundary condition. Investigations have been carried out under steady-state conditions. By comparing the present numerical solution and the experimental results, the method of

solution is confirmed. In general, the use of ferrofluids is efficient regarding heat transfer enhancement in helical coils, and the fluid temperature can be increased by 6 °C in the presence of magnetic field. Applying magnetic field gradient on the tube wall, Nusselt number increases by an increase in Reynolds number. The outlet temperature of water–Fe₃O₄ ferrofluid from the helical tube obeys the same trend as the Nusselt number. Using ferrofluids as working fluid and applying magnetic field can enhance the shear stress on the helical tube wall. Numerical results indicate that the magnetic gradient value has an optimum value concerning thermal–hydraulic performance. At low values of field strength, the increment of heat transfer rate and wall shear stress is high; however, a more moderate increase in Nusselt number can be seen at high values of the magnetic gradient. The shear stress growth at the higher values of strength is sharper and can diminish the heat transfer rise effects and decrease the thermal–hydraulic performance of helical tube.

References

- Chingulpitak S, Wongwiset S. Effects of coil diameter and pitch on the flow characteristics of alternative refrigerants flowing through adiabatic helical capillary tubes. *Int Commun Heat Mass Transf.* 2010;37(9):1305–11.
- Chingulpitak S, Wongwiset S. A comparison of flow characteristics of refrigerants flowing through adiabatic straight and helical capillary tubes. *Int Commun Heat Mass Transf.* 2011;38(3):398–404.
- Zhao Z, Wang X, Che D, Cao Z. Numerical studies on flow and heat transfer in membrane helical-coil heat exchanger and membrane serpentine-tube heat exchanger. *Int Commun Heat Mass Transf.* 2011;38(9):1189–94.
- Dravid AN, Smith K, Merrill E, Brian P. Effect of secondary fluid motion on laminar flow heat transfer in helically coiled tubes. *AIChE J.* 1971;17(5):1114–22.
- Kubair V, Kuloor N. Heat transfer to Newtonian fluids in coiled pipes in laminar flow. *Int J Heat Mass Transf.* 1966;9(1):63–75.
- Patankar SV, Pratap VS, Spalding DB. Prediction of laminar flow and heat transfer in helically coiled pipes. In: *Numerical prediction of flow, heat transfer, turbulence and combustion.* Amsterdam: Elsevier; 1983. p. 117–29.
- Xin R, Ebadian M. The effects of Prandtl numbers on local and average convective heat transfer characteristics in helical pipes. *J Heat Transf.* 1997;119(3):467–73.
- El-Genk MS, Schriener TM. A review and correlations for convection heat transfer and pressure losses in toroidal and helically coiled tubes. *Heat Transf Eng.* 2017;38(5):447–74. <https://doi.org/10.1080/01457632.2016.1194693>.
- Jamshidi N, Farhadi M, Ganji DD, Sedighi K. Experimental analysis of heat transfer enhancement in shell and helical tube heat exchangers. *Appl Therm Eng.* 2013;51(1):644–52.
- Kurnia JC, Sasmito AP, Mujumdar AS. Thermal performance of coiled square tubes at large temperature differences for heat exchanger application. *Heat Transf Eng.* 2016;37(16):1341–56. <https://doi.org/10.1080/01457632.2015.1136141>.
- Promthaisong P, Jedsadaratanachai W, Eiamsa-ard S. Numerical simulation and optimization of enhanced heat transfer in helical oval tubes: effect of helical oval tube modification, pitch ratio, and depth ratio. *Heat Transf Eng.* 2017. <https://doi.org/10.1080/01457632.2017.1384281>.
- Huminic G, Huminic A. Heat transfer characteristics in double tube helical heat exchangers using nanofluids. *Int J Heat Mass Transf.* 2011;54(19):4280–7.
- Huminic G, Huminic A. Heat transfer and entropy generation analyses of nanofluids in helically coiled tube-in-tube heat exchangers. *Int Commun Heat Mass Transf.* 2016;71:118–25.
- Jamshidi N, Farhadi M, Sedighi K, Ganji DD. Optimization of design parameters for nanofluids flowing inside helical coils. *Int Commun Heat Mass Transf.* 2012;39(2):311–7.
- Karami M, Akhavan-Behabadi MA, Fakoor-Pakdaman M. Heat transfer and pressure drop characteristics of nanofluid flows inside corrugated tubes. *Heat Transf Eng.* 2016;37(1):106–14. <https://doi.org/10.1080/01457632.2015.1042347>.
- Bhanvase BA, Sayankar SD, Kapre A, Fule PJ, Sonawane SH. Experimental investigation on intensified convective heat transfer coefficient of water based PANI nanofluid in vertical helical coiled heat exchanger. *Appl Therm Eng.* 2018;128:134–40. <https://doi.org/10.1016/j.applthermaleng.2017.09.009>.
- Hosseinzadeh M, Heris SZ, Beheshti A, Shanbedi M. Convective heat transfer and friction factor of aqueous Fe₃O₄ nanofluid flow under laminar regime. *J Therm Anal Calorim.* 2016;124(2):827–38. <https://doi.org/10.1007/s10973-015-5113-z>.
- Marin CN, Malaescu I, Fannin PC. Theoretical evaluation of the heating rate of ferrofluids. *J Therm Anal Calorim.* 2015;119(2):1199–203. <https://doi.org/10.1007/s10973-014-4224-2>.
- Khairul MA, Doroodchi E, Azizian R, Moghtaderi B. Advanced applications of tunable ferrofluids in energy systems and energy harvesters: a critical review. *Energy Convers Manag.* 2017;149:660–74. <https://doi.org/10.1016/j.enconman.2017.07.064>.
- Abbasi Z, Molaei Dehkordi A, Abbasi F. Numerical investigation of effects of uniform magnetic field on heat transfer around a sphere. *Int J Heat Mass Transf.* 2017;114:703–14. <https://doi.org/10.1016/j.ijheatmasstransfer.2017.06.087>.
- Rahman MM, Mojumder S, Saha S, Joarder AH, Saidur R, Naim AG. Numerical and statistical analysis on unsteady magnetohydrodynamic convection in a semi-circular enclosure filled with ferrofluid. *Int J Heat Mass Transf.* 2015;89:1316–30. <https://doi.org/10.1016/j.ijheatmasstransfer.2015.06.021>.
- Shafiei Dizaji A, Mohammadpourfard M, Aminfar H. A numerical simulation of the water vapor bubble rising in ferrofluid by volume of fluid model in the presence of a magnetic field. *J Magn Magn Mater.* 2018;449:185–96. <https://doi.org/10.1016/j.jmmm.2017.10.010>.
- Jafari A, Tynjälä T, Mousavi SM, Sarkomaa P. CFD simulation and evaluation of controllable parameters effect on thermomagnetic convection in ferrofluids using Taguchi technique. *Comput Fluids.* 2008;37(10):1344–53. <https://doi.org/10.1016/j.compfluid.2007.12.003>.
- Ghadiri M, Sardarabadi M, Pasandideh-fard M, Moghadam AJ. Experimental investigation of a PVT system performance using nano ferrofluids. *Energy Convers Manag.* 2015;103:468–76. <https://doi.org/10.1016/j.enconman.2015.06.077>.
- Sadeghinezhad E, Mehrali M, Akhiani AR, Tahan Latibari S, Dolatshahi-Pirouz A, Metselaar HSC, et al. Experimental study on heat transfer augmentation of graphene based ferrofluids in presence of magnetic field. *Appl Therm Eng.* 2017;114:415–27. <https://doi.org/10.1016/j.applthermaleng.2016.11.199>.
- Fadaei F, Molaei Dehkordi A, Shahrokh M, Abbasi Z. Convective-heat transfer of magnetic-sensitive nanofluids in the

- presence of rotating magnetic field. *Appl Therm Eng.* 2017;116:329–43. <https://doi.org/10.1016/j.applthermaleng.2017.01.072>.
27. Bahiraei M, Hangi M. Investigating the efficacy of magnetic nanofluid as a coolant in double-pipe heat exchanger in the presence of magnetic field. *Energy Convers Manag.* 2013;76:1125–33. <https://doi.org/10.1016/j.enconman.2013.09.008>.
 28. Mokhtari M, Hariri S, Barzegar Gerdroodbary M, Yeganeh R. Effect of non-uniform magnetic field on heat transfer of swirling ferrofluid flow inside tube with twisted tapes. *Chem Eng Process.* 2017;117:70–9. <https://doi.org/10.1016/j.ccep.2017.03.018>.
 29. Yarahmadi M, Moazami Goudarzi H, Shafii MB. Experimental investigation into laminar forced convective heat transfer of ferrofluids under constant and oscillating magnetic field with different magnetic field arrangements and oscillation modes. *Exp Thermal Fluid Sci.* 2015;68:601–11. <https://doi.org/10.1016/j.expthermflusci.2015.07.002>.
 30. Ahangar Zonouzi S, Khodabandeh R, Safarzadeh H, Aminfar H, Trushkina Y, Mohammadpourfard M, et al. Experimental investigation of the flow and heat transfer of magnetic nanofluid in a vertical tube in the presence of magnetic quadrupole field. *Exp Thermal Fluid Sci.* 2018;91:155–65. <https://doi.org/10.1016/j.expthermflusci.2017.10.013>.
 31. Asfer M, Mehta B, Kumar A, Khandekar S, Panigrahi PK. Effect of magnetic field on laminar convective heat transfer characteristics of ferrofluid flowing through a circular stainless steel tube. *Int J Heat Fluid Flow.* 2016;59:74–86. <https://doi.org/10.1016/j.ijheatfluidflow.2016.01.009>.
 32. Lajvardi M, Moghimi-Rad J, Hadi I, Gavili A, Dallali Isfahani T, Zabihi F, et al. Experimental investigation for enhanced ferrofluid heat transfer under magnetic field effect. *J Magn Magn Mater.* 2010;322(21):3508–13. <https://doi.org/10.1016/j.jmmm.2010.06.054>.
 33. Aminfar H, Mohammadpourfard M, Kahnamouei YN. Numerical study of magnetic field effects on the mixed convection of a magnetic nanofluid in a curved tube. *Int J Mech Sci.* 2014;78:81–90. <https://doi.org/10.1016/j.ijmecsci.2013.10.014>.
 34. Selimefendigil F, Öztöp HF, Chamkha AJ. Fluid–structure–magnetic field interaction in a nanofluid filled lid-driven cavity with flexible side wall. *Eur J Mech B/Fluids.* 2017;61:77–85.
 35. Selimefendigil F, Öztöp HF. Corrugated conductive partition effects on MHD free convection of CNT-water nanofluid in a cavity. *Int J Heat Mass Transf.* 2019;129:265–77. <https://doi.org/10.1016/j.ijheatmasstransfer.2018.09.101>.
 36. Selimefendigil F, Öztöp HF. Numerical study of natural convection in a ferrofluid-filled corrugated cavity with internal heat generation. *J Heat Transf.* 2016;138(12):122501.
 37. Selimefendigil F, Öztöp HF. Modeling and optimization of MHD mixed convection in a lid-driven trapezoidal cavity filled with alumina–water nanofluid: effects of electrical conductivity models. *Int J Mech Sci.* 2018;136:264–78.
 38. Selimefendigil F, Öztöp HF. Forced convection of ferrofluids in a vented cavity with a rotating cylinder. *Int J Therm Sci.* 2014;86:258–75.
 39. Selimefendigil F, Öztöp HF. Estimation of the mixed convection heat transfer of a rotating cylinder in a vented cavity subjected to nanofluid by using generalized neural networks. *Numer Heat Transf Part A Appl.* 2014;65(2):165–85. <https://doi.org/10.1080/10407782.2013.826109>.
 40. Selimefendigil F, Öztöp HF. Effect of a rotating cylinder in forced convection of ferrofluid over a backward facing step. *Int J Heat Mass Transf.* 2014;71:142–8. <https://doi.org/10.1016/j.ijheatmasstransfer.2013.12.042>.
 41. Selimefendigil F, Öztöp HF. Analysis of MHD mixed convection in a flexible walled and nanofluids filled lid-driven cavity with volumetric heat generation. *Int J Mech Sci.* 2016;118:113–24. <https://doi.org/10.1016/j.ijmecsci.2016.09.011>.
 42. Selimefendigil F, Öztöp HF, Abu-Hamdeh N. Mixed convection due to rotating cylinder in an internally heated and flexible walled cavity filled with SiO₂–water nanofluids: effect of nanoparticle shape. *Int Commun Heat Mass Transf.* 2016;71:9–19. <https://doi.org/10.1016/j.icheatmasstransfer.2015.12.007>.
 43. Ito H. Friction factors for turbulent flow in curved pipes. *Trans ASME J Basic Eng D.* 1959;81:123–34.
 44. Aminfar H, Mohammadpourfard M, Mohseni F. Two-phase mixture model simulation of the hydro-thermal behavior of an electrical conductive ferrofluid in the presence of magnetic fields. *J Magn Magn Mater.* 2012;324(5):830–42.
 45. Rosensweig RE. *Ferrohydrodynamics*. North Chelmsford: Courier Corporation; 2013.
 46. Shercliff JA. *A textbook of magnetohydrodynamics*. Applied electricity and electronics division-The Commonwealth and international library. Oxford: Pergamon Press; 1965.
 47. Tzirtzilakis E. A mathematical model for blood flow in magnetic field. *Phys Fluids.* 2005;17(7):077103.
 48. Khanafer K, Vafai K, Lightstone M. Buoyancy-driven heat transfer enhancement in a two-dimensional enclosure utilizing nanofluids. *Int J Heat Mass Transf.* 2003;46(19):3639–53.
 49. Hamilton RL, Crosser O. Thermal conductivity of heterogeneous two-component systems. *Ind Eng Chem Fundam.* 1962;1(3):187–91.
 50. Mahmoudi AH, Pop I, Shahi M, Talebi F. MHD natural convection and entropy generation in a trapezoidal enclosure using Cu–water nanofluid. *Comput Fluids.* 2013;72:46–62.
 51. Aminfar H, Mohammadpourfard M, Kahnamouei YN. A 3D numerical simulation of mixed convection of a magnetic nanofluid in the presence of non-uniform magnetic field in a vertical tube using two phase mixture model. *J Magn Magn Mater.* 2011;323(15):1963–72.
 52. Bilen K, Yapici J, Celik C. A Taguchi approach for investigation of heat transfer from a surface equipped with rectangular blocks. *Energy Convers Manag.* 2001;42:10.